Electrochemical formation of four Al-Li phases (β-AlLi, Al_2Li_3, $AlLi_{2-x}$, Al_4Li_9) at intermediate temperatures

Ghavidel, Mohammadreza Zamanzad; Kupsta, Martin R.; Le, Jon; Feygin, Eliana; Espitia, Andres; Fleischauer, Michael D.

Publisher's version / Version de l'éditeur:
https://doi.org/10.1149/2.0061916jes
Journal of The Electrochemical Society, 166, 16, pp. A4034-A4040, 2019-12-03

Electrochemical Formation of Four Al-Li Phases (β-AlLi, Al_2Li_3, $AlLi_{2-x}$, Al_4Li_9) at Intermediate Temperatures

Mohammadreza Zamanzad Ghavidel,[1] Martin R. Kupsta,[1,a] Jon Le,[2,b] Eliana Feygin,[2] Andres Espitia,[2] and Michael D. Fleischauer [1,2,*,z]

[1] *Department of Physics, University of Alberta, Edmonton AB T6G 2E1, Canada*
[2] *National Research Council - Nanotechnology Research Centre, Edmonton AB T6G 2M9, Canada*

Aluminum electrodes have been considered for use in lithium and lithium ion batteries for nearly four decades. Although the Al-Li equilibrium phase diagram contains multiple Al-Li phases, only β-AlLi forms during room temperature cycling. Al_2Li_3 can be formed when electrochemically inserting Li at temperatures above 400°C, and Al_4Li_9 is occasionally detected after extended room temperature cycling. Here, four equilibrium phases of Al-Li (β-AlLi, Al_2Li_3, $AlLi_{2-x}$, Al_4Li_9) were produced by the electrochemical lithiation and delithiation of 1100-series aluminum foil at moderate to intermediate temperatures (30–150°C) using a carbonate-based electrolyte. Phase identification was performed using ex-situ X-ray diffraction and coulometry, after accounting for the consumption of lithium in electrolyte breakdown products. After overcoming an initial nucleation barrier, β-AlLi formed at all temperatures, Al_2Li_3 and $AlLi_{2-x}$ formed at temperatures above 60°C at moderate rates, and above 35°C at low rates, and Al_4Li_9 formed at temperatures above 100°C. All expected phases were also encountered during delithiation. The effects of nucleation and diffusion on observed phases and capacities are also discussed.

 [DOI: 10.1149/2.0061916jes]

Manuscript submitted October 8, 2019; revised manuscript received November 12, 2019. Published December 3, 2019.

Lithium-ion batteries are the dominant energy storage technology for applications ranging from portable devices to electric vehicles.[1–3] Performance improvements, such as lower costs, higher capacities, and safer systems, depend on advanced materials and insight, including improved electrode materials. There are five broad approaches to negative electrode materials - using lithium metal,[4] intercalation materials (i.e. graphite),[5] lithium-metal alloys,[2,6] conversion materials,[7] or no active material at all.[8] Lithium metal foil has specific and volumetric capacities of 3860 mAh g^{-1} and 2061 mAh cm^{-3}, respectively. Repeated stripping and plating of lithium produces dendrites which lead to serious safety concerns such as short circuits and fires.[4,9] In most conditions, dendrites do not form on graphite intercalation electrodes as the lithium is hosted in specific sites. Improved safety comes with the cost of more limited specific and volumetric capacities (∼370 mAh g^{-1} and ∼840 mAh cm^{-3}, respectively).[10–12] Conversion materials such as lithium titanate further strengthen safety at the cost of capacity (∼175 mAh g^{-1} and ∼612 mAh cm^{-3}), and cell energy density (∼30% lower).[13,14] Safe, low cost, high capacity negative electrode materials are required for continued advancement of the field.

Metal alloy negative electrodes offer the potential of high capacities at low cost.[2,6,15] Alloy negative electrodes such as Li-Si,[6,15] Li-Sn,[6,15] and Al-Li[16–18,20] have been studied extensively. Complete lithiation of Sn should lead to specific and volumetric capacities of ∼1000 mAh g^{-1} and ∼2100 mAh cm^{-3}, respectively, nearly triple the capacity of graphite. The lithiation of Sn proceeds as expected from the equilibrium phase diagram at temperatures near 400°C,[6,21] but at room temperature, crystalline phases are only detected for $x > 2.5$ in Li_xSn.[22,23] Phases such as Li_7Sn_2, $Li_{13}Sn_5$, and $Li_{17}Sn_4$ (sometimes identified as $Li_{22}Sn_5$) are not well defined, thought to be due to low atom mobility in phases with high melting points.[6]

Electrochemical lithiation of aluminum follows a similar trend. Based on the Al-Li equilibrium phase diagram,[24] four different phases of Al-Li, namely β-AlLi, Al_2Li_3, $AlLi_{2-x}$, and Al_4Li_9 (specific and volumetric capacities of 2250 mAh g^{-1} and ∼1850 mAh cm^{-3}, respectively) are expected to form. However, the vast majority of published research on the lithiation of Al only reports the formation of β-AlLi.[6,12,25,26] Notable exceptions include lithiations performed at temperatures above 400°C using molten salt electrolytes (to form Al_2Li_3[27,28] and Al_4Li_9[28]) or forming Al_2Li_3 and Al_4Li_9 after extended cycling.[18,29] We are unaware of any previous reports on the electrochemical formation or dissociation of $AlLi_{2-x}$. Equilibrium phases of Li-Sn that may not be electrochemically accessible were justified based on limited atom mobility in high-melting point alloys (>700°C for $Li_{13}Sn_5$ or Li_7Sn_2). Al_2Li_3 melts at ∼ 500°C; $AlLi_{2-x}$ and Al_4Li_9 melt near 300°C.[24] A more complete and quantifiable explanation of the discrepancy between equilibrium and electrochemically-accessible phases is needed.

Aluminum-based electrodes are promising,[19] but typically exhibit capacity fade. Theories explaining Al-Li capacity fade include volume changes leading to pulverization; formation of inactive Al-Li-O on particle surfaces; and formation of irreversible Li-rich phases or the trapping of Li in Al electrodes.[20,30–34] Electrolyte degradation may also have a significant influence on observed phases.[12,30] Comprehensive ex- and in-situ studies by Qin et al.[12,30] suggest that Li-rich phases (i.e. beyond β-AlLi) formed but X-ray diffraction results were not conclusive. Reports demonstrating the formation of Al_4Li_9 after long term cycling,[18] i.e. trapping Li, only showed the 'standard' potential plateau associated with the α-AlLi/β-AlLi phase transition, and the reversible capacity associated with Al (i.e. excluding capacity from components like carbon) peaked at 800 mAh g^{-1}. Here, we provide correlated electrochemical and structural data to clarify the electrochemical Al-Li reaction pathway and facilitate further investigations in to capacity fade of aluminum-based alloys.

Reaction pathways are temperature-dependent. Commercial 18650 lithium-ion cells are typically limited to moderate temperatures (e.g. 45°C charging, 60°C discharging, 50°C storage).[35] Specialized lithium-ion cells used in high-value applications like measurement-while-drilling[36] are capable of hundreds of cycles at temperatures above 100°C.[37] Challenges and opportunities with high temperature energy storage are described elsewhere.[38,39] Room to elevated temperature cycling is used here to separate the effects of slow diffusion from nucleation barriers.

We developed an electrochemical test platform to study lithium-ion electrode and electrolyte materials in operation at temperatures up to 400°C.[40] Preliminary studies using sputter-deposited aluminum thin films (500 nm thick) showed that electrochemical cycling at 110°C led to sharply higher capacities and multiple potential plateaus, indicative

*Electrochemical Society Member.
[a]Present address: Micralyne Inc., Edmonton, Alberta T6N 1E6 Canada.
[b]Present address: Interface Fluidics, Edmonton, Alberta T6G 1V6 Canada.
[z]E-mail: michael.fleischauer@nrc.ca

of co-existing Al-Li phases. The nominal capacity, 7000 mAh g^{-1}, is beyond that of any expected Li-metal phase and the extra capacity of ~5000 mAh g^{-1} was likely due to a large amount of electrolyte breakdown. Here we present a thorough investigation of Al-Li phase formation between 30 to 150°C using thick aluminum foil electrodes.

Experimental

Aluminum electrodes were fabricated by punching 12.7 mm dia. disks from 0.013 mm thick pieces of 1100-series aluminum foil (99% purity, McMaster-Carr, Aurora, OH USA). Aluminum was both the active material and current collector - no binders or substrates were used. Electrodes were cleaned by immersion first in acetone for 15 minutes, then in isopropyl alcohol for another 15 minutes, then dried at 60°C in an oven for 1 hour before transfer to the glove box described below. No other modifications were performed to the aluminum foil.

All electrochemical testing was performed using high-temperature Conflat cells, as described elsewhere.[40] All Conflat cells were assembled in an Ar-filled glove box maintained at <5 ppm H_2O and O_2. Lithium electrodes were fabricated by punching 17.5 mm dia. disks from 0.1 mm (0.004") thick strips of brushed Li metal (Rockwood Lithium, Charlotte, NC USA). The stack pressure was constant for all samples at 0.8 MPa. Whatman GF/A glass filters (Fisher Scientific, Hampton, NH USA) were used as the cell separators. Cell electrolyte consisted of approximately 200 μL of 1 M $LiN(SO_2CF_3)_2$ (99.95%, Sigma-Aldrich) dissolved in ethylene carbonate (99%, Sigma-Aldrich): propylene carbonate (99.7%, anhydrous, Sigma-Aldrich) 1:1 vol.:vol. Electrolyte salt was used as provided. Electrolyte solvents and the combined electrolyte were dried using activated 3A and 4A molecular sieves.

Electrochemical cycling was performed on a lab-built multichannel system with integrated temperature control, as described previously.[40] Each cell was held at open circuit while being heated to the indicated temperature at a rate of 30°C/hour. Cell temperatures were then held within 1°C of the indicated temperature for the duration of the electrochemical testing, unless otherwise indicated. The current was held constant at ±160 μA (0.036 mA g^{-1}, 0.126 mA cm^{-2}) for all samples, unless otherwise indicated; ±160 μA corresponds to approximately C/30 if β-AlLi is considered as the fully lithiated phase. Cycling was performed at ±40 μA (0.009 mA g^{-1}, 0.032 mA cm^{-2}) for a few samples (as indicated). Voltage limits are described in the text. Data was collected approximately every 20 seconds over the duration of each test. Differential capacity vs. potential curves were obtained by performing linear least square fits on three capacity-potential data points separated in potential by at least 0.5 mV.

Cyclic voltammetry was performed to measure electrolyte stability as a function of temperature. Cyclic voltammograms were collected from cells without an aluminum electrode between 0.001 V and 1.000 V vs. Li/Li^+ at rates of 1.0, 0.3, 0.1, and 1.0 mV s^{-1} at 30, 60, 90, 120, 135, and 150°C. Cell potential was controlled with a Biologic BCS-805. Cell temperature was controlled with the aforementioned lab-built system. Cells were maintained at 1.0 V vs. Li/Li^+ for 1 hour before and after each series of potential sweeps.

Samples were prepared for X-ray diffraction (XRD) by disassembling cycled Conflat cells in the glove box described above and transferring the cycled electrode to an encapsulated sample holder. Encapsulated holders were fabricated by punching a 15.9 mm dia. hole in a piece of 0.25 mm thick Teflon double-sided adhesive tape (McMaster) and sandwiching the Teflon (and sample) between a standard glass slide and a 0.05 mm (0.002") thick layer of polypropylene film (see Figure S1). Brushed lithium foil stored in such an encapsulated holder maintains its luster for many days outside of the glove box. All XRD data collection was performed within two hours of the encapsulated sample holder being removed from the glove box.

XRD was performed using a Bruker D8-Discover diffractometer with Cu K_α radiation (50 kV, 1000 μA; $\lambda = 1.5406$ Å) equipped with a Vantec 500 area detector. Scattering patterns were collected between 10 and 105 degrees scattering angle in total, based on five 2D XRD frames spaced by 20 degrees scattering angle with acquisition times of 2 minutes per frame. XRD patterns presented here are the integrated intensities extracted from 2D frames using Eva software.

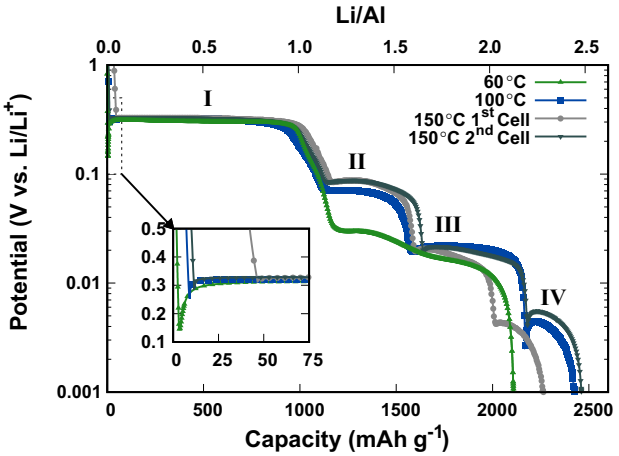

Figure 1. Potential vs. capacity curves for Al-Li cells cycled at three different temperatures. Potentials are shown using a logarithmic scale on the main plot and a linear scale on the inset. Capacities are provided in mAh g^{-1} on the lower axis and as a ratio of Li/Al on the top axis. Plateau regions are indicated with Roman numerals (I-IV).

Results and Discussion

Potential vs. capacity data from Al-Li cells cycled to 0.001 V vs. Li/Li^+ at three different temperatures are provided in Figure 1. Several potential plateaus were observed during lithiation; four distinct regions (I, II, III, and IV) are indicated in Figure 1. The first plateau at 0.3 V vs. Li/Li^+ was preceded by a sharp, temperature-dependent drop shown in the inset of Figure 1. Cells cycled near 60°C exhibited nucleation barriers of hundreds of mV; cells cycled near 100°C exhibited nucleation barriers of tens of mV, and cells cycled near 150°C exhibited nucleation barriers of a few mV. This behavior is characteristic of a nucleation process, with the additional potential providing the additional energy required to overcome the nucleation barrier associated with the formation of a new crystalline phase.[18,41] In addition, the inset in Figure 1 shows that the slope of the potential vs. capacity curve changed as the temperature increased. The shallower slopes in data collected at temperatures above 60°C indicates that more Li was inserted before a new phase nucleated. The higher content of Li atoms in the solid solution structure (usually identify as α-AlLi) made nucleation of the next phase easier and reduced the nucleation barrier at higher temperatures.

No appreciable capacity for lithium was observed for foil samples cycled at 30°C at ±160 μA. This is consistent with previous reports of similar Al foil electrodes, which required modification to remove the surface oxide (e.g. polishing under Argon,[42] removing the surface oxide electrochemically[43] or etching the foils[44]) for room temperature electrochemical activity. Cycling at higher temperatures likely provides sufficient energy for lithium to break through the oxide layer without removing it.

The potential of the first plateau (region I) was approximately constant at 0.3 V vs. Li/Li^+ to capacities of approximately 1000 mAh g^{-1} (Figure 1). All three curves displayed sharp potential drops shortly thereafter. This plateau is commonly reported in investigations of Al-Li electrodes,[25,27,41,44–49] and attributed to the formation of β-AlLi (theoretical capacity 993 mAh g^{-1}).[25,44,45] Any small differences in capacity could be due to incomplete lithiation, variations in roughness of the Al foils, or the formation of solid-electrolyte interphases (SEI). The transition between regions I and II added approximately 100 mAh g^{-1}.

Formation of the second plateau in Figure 1 (region II) added approximately 500 mAh g^{-1} at all temperatures tested. Data collected at 100 and 150°C dropped in potential quickly near capacities of

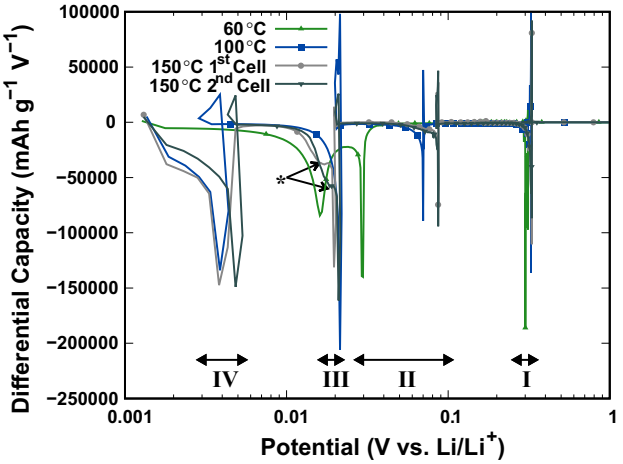

Figure 2. Differential capacity curves for Al-Li cells cycled at three different temperatures. Plateau regions from Figure 1 are indicated with Roman numerals (I-IV). Arrows and a star indicate an extra peak in the 150°C data sets.

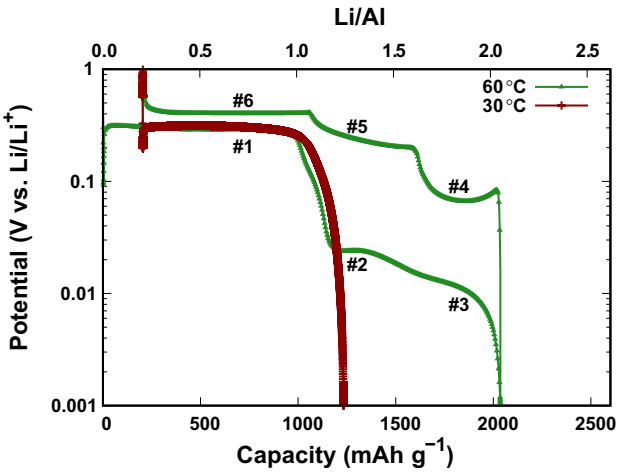

Figure 3. Potential vs. capacity curves for the Al foil cycled at 60°C then lithiated at 30°C to 0.001 V vs. Li/Li$^+$. Capacities are provided in mAh g^{-1} on the lower axis and as a ratio of Li/Al on the top axis.

1600 mAh g^{-1}; data collected at 60°C declined slowly between 1300 and 1600 mAh g^{-1}. The potential of the second plateau varied, from 0.09 V at 150°C to 0.07 V at 100°C to 0.03 V vs. Li/Li$^+$ at 60°C. This could be partially due to changes in overall cell resistance (mostly ionic resistance) at different temperatures, but given the low current density a large iR voltage drop is unlikely, especially a drop large enough to explain the measured potential at 60°C. An alternate explanation involving the formation of different alloy mixtures or intermediate phases with a higher Li content at different temperatures is provided later in the manuscript.

Capacity variations with temperature were small for regions I and II. Capacity additions in region III varied between 400 and 600 mAh g^{-1}. Data collected at 60°C exhibited a slow decay in potential followed by a sharp drop to 0.001 V and the end of the half cycle. Data collected at 100 and 150°C exhibited a nucleation barrier of a few mV between regions II and III, followed by a slow decay and sharp drop in potential to the next nucleation barrier between regions III and IV. Two different data sets for 150°C are shown in Figure 1, indicating that there was ∼10% capacity variation between samples at higher temperatures, especially at 150°C. However, the capacities of both cells at 150°C were lower than data collected at 100°C in region III. Thermodynamically, the formation of a given Al-Li alloy should become easier as the temperature increases and more complete lithiation is to be expected. This apparent discrepancy is addressed later.

The fourth and final plateau was only observed for data collected at 100 and 150°C. In both cases the additional capacity was approximately 250 mAh g^{-1}. The nucleation barrier for data collected at 100°C was more prominent than at 150°C but only amounted to a few mV.

Differential capacity curves based on the data in Figure 1 are shown in Figure 2. Positive differential capacity values are due to the nucleation phenomenon and negative peaks are due to the potential plateaus. Peaks are grouped in to four regions (I - IV) corresponding to the four plateaus in Figure 1. Three peaks are present in the data collected at 60°C. The first peak (region I) was due to the nucleation process of the Al-Li phase followed by the potential plateau. The second and third peaks were due to the formation of potential plateaus without nucleation phenomena. Both of these peaks were shifted to lower potentials, specifically the second peak which moved significantly. As discussed previously, a large iR drop is unlikely; at ±160 μA, every 10 mV difference implies an additional 60 Ω series resistance, which is very unlikely across a ∼13 μm thick metallic electrode. The voltage shift at 60°C is therefore likely due to phase nucleation barriers, slow Li diffusion and formation of a concentration gradient, or formation of an intermediate phase that does not appear at 100 or 150°C.

Four peaks are apparent in the 100°C differential capacity data provided in Figure 2. The additional (fourth) peak was caused by nucleation and formation of the last potential plateau in Figure 1. At this temperature, all four peaks showed nucleation phenomena. Increasing the temperature to 150°C led to the formation of a fifth peak indicated with an arrow and star in Figure 2. Different potentials (2 to 0.25 V vs. Li/Li$^+$) have been reported previously for the beginning of the SEI layer formation, influenced by the electrolyte, type of electrodes, and current density.[50] While there was likely some SEI formation at higher potentials, the broad peaks near 20 mV vs. Li/Li$^+$ in the 150°C data suggest SEI formation is most prominent at this potential.

Electrolyte stability was investigated using cyclic voltammetry; data is provided in Figure S2. The electrolyte was stable at 30, 60, and 90°C for all sweep rates tested. Some electrolyte breakdown is noticeable at 120°C at 0.1 mV s^{-1}, but the breakdown is less prominent in the cyclic voltammograms collected at 135 or 150°C. One would expect faster breakdown at higher temperatures, which was not observed above 120°C. This may be due to SEI buildup and a less reactive surface; testing with a different thermal history (e.g. first increasing the temperature to 150°C, then performing cyclic voltammetry at successively lower temperatures) may produce the expected results. Some of the reduced Al-Li cell performance at 150°C can be assigned to electrolyte breakdown (or breakdown of electrolyte impurities). Although the electrolyte is not ideal, it is at least adequate for the studies of Al-Li reactions described here.

As previously discussed, direct lithiation of the Al foil at 30°C was not possible without modifying the surface of the foils. Potential vs. capacity data from an Al foil lithiated/delithiated at 60°C and then lithiated at 30°C is shown in Figure 3. Three Al-Li reactions were likely reversible at 60°C as three potential plateaus (#1 to #3 in Figure 3) are apparent during insertion and three (#4 to #6) in removal. This supports ascribing the three differential capacity peaks at 60°C, especially the broad peak at 0.018 V vs. Li/Li$^+$, to the growth of a Al-Li phase and not to SEI (broad differential capacity peaks at 0.02 V for data collected at 150°C are assigned to SEI formation). The nucleation barrier was also observed during delithiation as a maximum before formation of the plateaus.

Overall insertion and removal capacities at 60°C were ∼2000 mAh g^{-1} and ∼1800 mAh g^{-1}, respectively. There are small variations between insertion and removal capacities for what likely should be symmetric plateaus (e.g. insertion/removal for #1/#6, #2/#5, and #3/#4) but the overall trend is apparent. Plateaus #4 and #5 appear somewhat longer than expected, and plateau #6 somewhat shorter. The ∼200 mAh g^{-1} of irreversible capacity can likely be attributed to a combination of SEI formation, electrode pulverization, and trapped lithium.

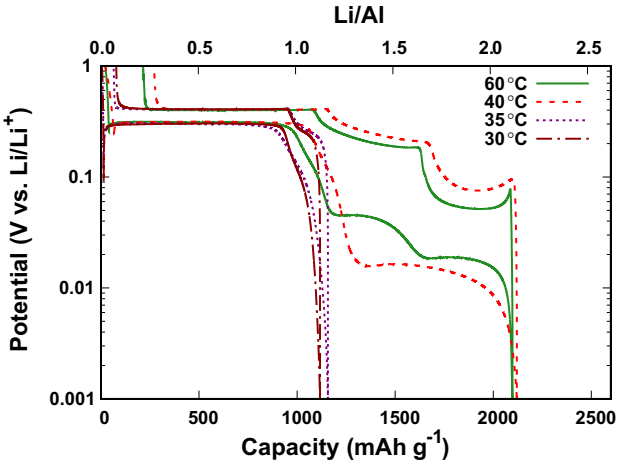

Figure 4. Potential vs. capacity curves for Al foils cycled at ±40 μA (~C/120) to 0.001 V vs. Li/Li^+. Temperatures are indicated. Capacities are provided in mAh g^{-1} on the lower axis and as a ratio of Li/Al on the top axis.

Approximately 1000 mAh g^{-1} of lithium was inserted after cooling the cell cycled at 60°C to 30°C. This continues the trend of higher temperatures being required to observe more plateaus (i.e. one plateau at 30°C, three plateaus at 60°C, four plateaus at 100°C). Formation of the first plateau at 30°C was likely facilitated by the presence of residual lithium or disruption of the surface oxide. The nucleation barrier at 30°C compared to the first cycle at 60°C was decreased (Figure 3) and it was drastically lower than the potential required for nucleation at 30°C (where no nucleation was observed). However, regions II - IV were not observed.

Nucleation barriers will vary as function of test conditions, including current density and temperature. Very low rate testing (±40 μA, approximately C/120 if β-AlLi is considered as the fully lithiated phase) was performed at intermediate temperatures; data from cells heated to 30, 35, 40, or 60°C is provided in Figure 4. Data collected at 30 and 35°C is typical of previous room temperature investigations of Al-Li; a single plateau extending to approximately 1000 mAh g^{-1}, followed by a rapid drop in cell potential (denoted here as region I). Cell capacity approximately doubles to over 2000 mAh g^{-1} for cells cycled at 40 or 60°C. Regions II and III are apparent in the 60°C data, and based on the capacity, are also present at 40°C. Formation of regions II and III are linked and highly temperature dependent. Plateaus in removal data suggest small amounts of region II may be present at 30 and 35°C.

Features in region I can be likely assigned to the nucleation and growth of β-AlLi based on measured capacities and decades of research. Phase identification in regions II-IV requires additional characterization. Diffraction patterns collected after lithiating the Al foils to 0.001 V vs. Li/Li^+ at different temperatures are presented in Figure 5. Reference peak positions are provided below each scattering pattern, using data from JCPDS cards 04-0787 (Al), 03-1215 (AlLi), 26-1008 (Al_2Li_3), 1-79-8685 ($AlLi_{2-x}$) and 24-0089 (Al_4Li_9). At 30°C, only β-AlLi and two residual Al peaks (indicated by stars) are observed. Therefore, region I in Figures 1 and 2, and plateau #1 in Figure 3, are due to a co-existing low Li-content Al phase (Al or more likely α-AlLi) and β-AlLi. α-AlLi is a solid solution phase with an expected Li content of less than 1% near room temperature,[24] and as a solid solution should not have a nucleation barrier. Nucleation barriers observed at low capacities are therefore assigned to the nucleation of β-AlLi. Nucleation of β-AlLi was strongly temperature and current dependent - nucleation barriers were at least 0.3 V at 30°C and moderate current density; 0.2 V at 30°C and very low current density, 0.15 V at 60°C and moderate current density, and 0.05 V at 60°C at very low current density (see Figures 1 and 4). Investigations of nucleation barriers as a function of composition, test conditions, and sample morphology are being pursued.

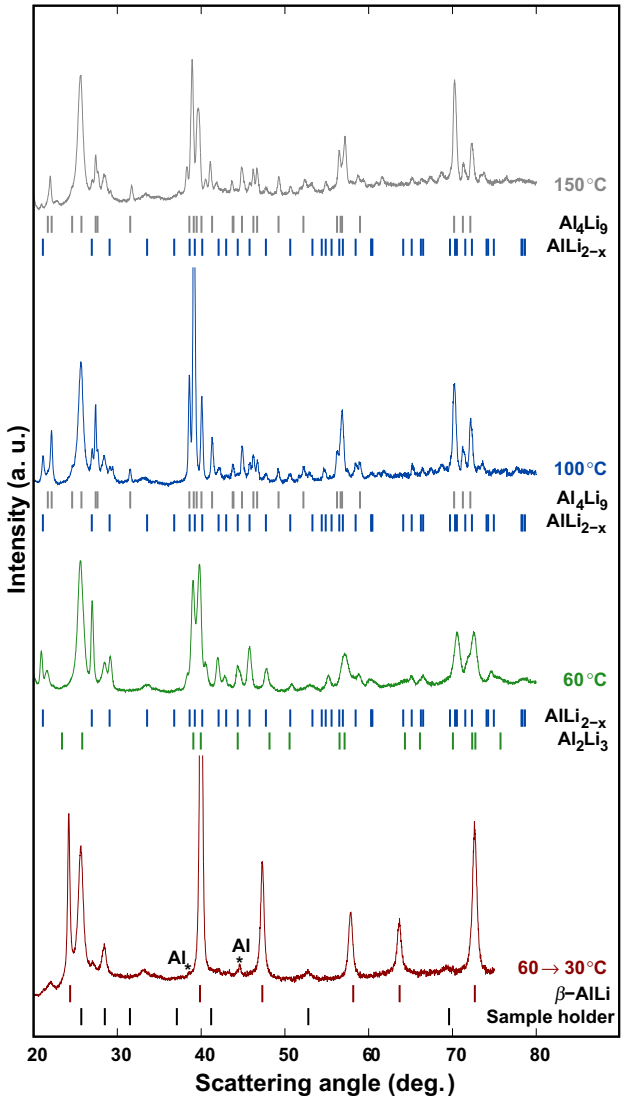

Figure 5. XRD patterns collected on samples lithiated to 0.001 V vs. Li/Li^+ at different temperatures (as indicated). Peak positions from reference patterns and the sample holder are indicated and described in the text.

At higher lithiation temperatures, XRD patterns became more complex, generally consisting of two Al-Li phases; residual peaks of Al were not observed. At 60°C a mixture of peaks characteristic of Al_2Li_3 and $AlLi_{2-x}$ were observed. For samples tested at 100 and 150°C, peaks characteristic of $AlLi_{2-x}$ and Al_4Li_9 were observed. One can infer that regions II, III, and IV are due to co-existing β-AlLi and Al_2Li_3, Al_2Li_3 and $AlLi_{2-x}$, and $AlLi_{2-x}$ and Al_4Li_9, respectively. Mixtures of phases such as $Al_2Li_3/AlLi_{2-x}$ (60°C) or $AlLi_{2-x}/Al_4Li_9$ (100, 150°C) at nominally full lithiation (1 mV vs. Li/Li^+) illustrate that phase transformations at the selected temperatures and current density were not complete. While lithiation at a lower rate may lead to more complete alloying, it should be noted that these tests were performed at very low rates (~C/70) and at high temperatures, two approaches to mitigate slow diffusion. However, very slow diffusion, even at high temperatures, may be the underlying cause. Residual Al-Li phases have been observed by others[18,28,29] and are consistent with the trapping of Li.[28,29] Self-discharge during transfer of partially delithiated samples for XRD[18] could also result in mixed phases. The Conflat cells used here are straightforward to disassemble - cycled electrodes can be extracted by removing four bolts and lifting out the relevant cell components. Short circuits during assembly or disassembly are very unlikely as the cell electrodes are laterally surrounded by

glass (see Figure 1 in Ref. 40). Mixed phases at nominally full lithiation are therefore ascribed to very slow diffusion. Efforts to quantify diffusion rates as a function of temperature and composition are underway.

Two changes can be noted when inserting and removing Li at 150°C compared to lower temperatures. First, more complete formation of Al_4Li_9 was observed. Second, consistent delithiation of samples at 150°C was not observed, although near-complete delithiation was regularly observed at lower temperatures (30, 60 and 100°C). Earlier studies[41,51,52] have shown that the mechanical stability of Al-Li alloys decreases as more Li is incorporated, which may result in a higher degree of pulverization. It should be noted that these samples are by most standards very thick. Capacities of >2000 mAh g^{-1} (>7 mAh cm^{-2}, higher than in most commercial lithium-ion cells) were obtained from solid 13 μm thick foil electrodes without any binder or intentional porosity. A practical reason may be limited stack pressure; Li melts at 181°C and may not be able to maintain sufficient pressure/electrical contact at 150°C. Capacity fluctuations at 150°C are therefore not surprising.

All features present in electrochemical and structural data at 150°C were also observed at 100°C. Results from reversible phase transformations at 100°C are presented in Figure 6. Potential vs. capacity data from samples lithiated/delithiated to specific potentials at 100°C are shown in Figure 6a). In these experiments, each sample was separately lithiated from open circuit potential to either the specified potential, or first lithiated until 0.001 V vs. Li/Li^+ and then delithiated to the specified potential. Each sample was then extracted from the cell and subjected to ex-situ XRD. Sample-to-sample variability was low; data from the first four cells overlap within 20 mAh g^{-1} to 0.03 V vs. Li/Li^+. Variation increased in region III to approximately 50 mAh g^{-1}, as noted previously.

XRD diffraction patterns in Figure 6b illustrate that the Al foil lithiated up to 0.2 V transformed almost completely to β-AlLi, as expected. Two additional weak peaks from Al are also apparent, as in Figure 5. Next, at 0.035 V Al_2Li_3 was detected with some residual β-AlLi, confirming that the second plateau (region II) was due to the formation of Al_2Li_3 and co-existing β-AlLi and Al_2Li_3. As the potential dropped to 0.005 V vs. Li/Li^+, β-AlLi disappeared and $AlLi_{2-x}$ was detected along with a few weak peaks from Al_2Li_3. The third plateau (region III) is therefore due to coexisting Al_2Li_3 and $AlLi_{2-x}$. Finally, as the potential decreased to 0.001 V, Al_2Li_3 could not be detected and Al_4Li_9 appeared. During delithiation to 0.04 V vs. Li/Li^+, $Al_4Li_9/AlLi_{2-x}$ transformed to predominantly $AlLi_{2-x}$ and at 0.1 V vs. Li/Li^+, Al_2Li_3 was predominant. Finally, at 0.3 V vs. Li/Li^+ the electrode was again β-AlLi. Phase transformations were not complete at step-changes in potentials below 0.2 V vs. Li/Li^+, consistent with the data in Figure 5. However, at 0.2 V during lithiation and 0.3 V during delithiation only β-AlLi was detected, suggesting all phase transformations are reversible. XRD patterns collected before and after a complete cycle (from open circuit to 1 mV to 1 V vs. Li/Li^+) at 100°C are shown in Figure S3. Peak height differences are due to preferential orientation of the grain in as-received Al foils and lithiated/delithiated foils.

XRD patterns for samples lithiated and delithiated at 60 and 150°C are presented in Figure S4 and Figure S5, respectively. Results presented here confirm the reversible formation of β-AlLi, Al_2Li_3, $AlLi_{2-x}$ and Al_4Li_9 in regions I, II, III and IV, respectively.

Potential vs. capacity data collected at 100°C superimposed on the equilibrium Al-Li phase diagram is shown in Figure 7. Changes in potential occur at compositions similar to the phase transitions, but some deviations are apparent. Deviations are most prominent below 0.02 V vs. Li/Li^+. While the rate of electrochemical (de)lithiation should affect the apparent phase boundaries, slow diffusion would shift phase transitions to lower Li/Al compositions than expected (i.e. incomplete lithiation). Here, apparent phase boundaries are at more Li-rich compositions. Electrochemical testing at high temperatures with organic electrolytes leads to significant electrolyte breakdown - in some cases, breaking down enough electrolyte to be visible to the naked eye (see Figure 7 of Ref. 40). The overall insertion capacity

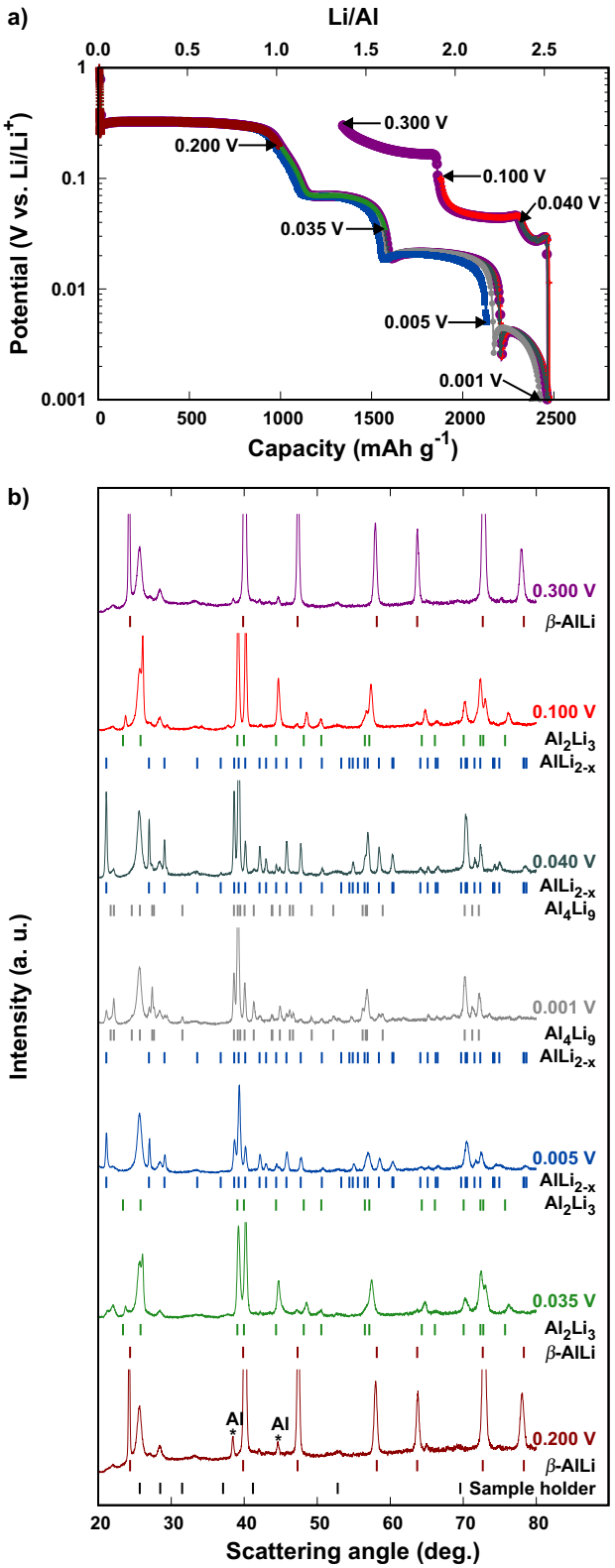

Figure 6. a) Potential vs. capacity curves for Al-Li cells cycled at 100°C to specific potentials (as indicated). Results provided here were collected from seven cells, each cycled from open circuit to the indicated potential. b) XRD patterns from samples cycled to the indicated potential.

(2.3 Li/Al) corresponds with the expected capacity of Al_4Li_9 (2.25 Li/Al), but, as noted previously, complete formation of Al_4Li_9 was not observed. Additional capacity of ~0.3 Li/Al can therefore be assigned to SEI formation.

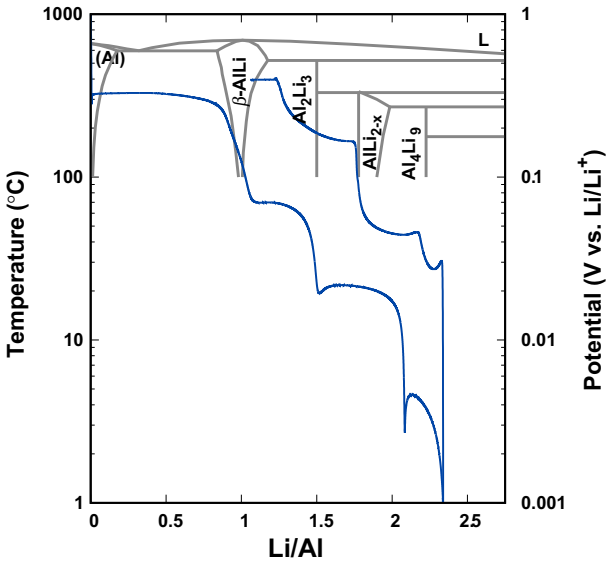

Figure 7. Phase diagram of Al-Li (gray, adapted from Ref. 24, left axis) and cell potential versus Li/Al ratio collected at 100°C (blue, right axis).

Phase transitions on delithiation occur at more Li-rich compositions than on lithiation. The shift is approximately consistent at ~0.3 Li/Al (see Figure 7). If one assumes limited pulverization, reversible phase transitions can therefore be used to quantify SEI formation as a function of cycling conditions (e.g. temperature, potential, duration) by assuming lithium goes in and out of the electrode but only in to the SEI. Although extended (or even limited) cycling is not the focus here, first cycle irreversible capacities varied between 0.2 and 0.8 Li/Al, lower at lower temperatures (e.g. see Figure 3) and higher at higher temperatures, depending on the degree of lithiation (not shown). The effects of current density (on repeated cycling and duration at temperature) area being investigated separately.

Correlation between the electrochemical and equilibrium thermal phase transitions is strong, even including the extended range of β-AlLi at higher temperatures, as suggested by the inset data of Figure 1. Electrochemical testing may also provide a route to detect new (potentially metastable) phases; $AlLi_{2-x}$ was only identified in 2010,[24,53] after decades of research on Al-Li alloys (for energy storage and structural applications).

Conclusions

High temperature compatible Conflat cells and ex-situ XRD were used to identify phases formed during the electrochemical lithiation and delithiation of aluminum foils. Large potentials were required to nucleate β-AlLi at lower temperatures. At intermediate temperatures (>35°C) three and at high (>90°C) four reversible phases of Al-Li (β-AlLi, Al_2Li_3, $AlLi_{2-x}$ and Al_4Li_9) were detected via electrochemical and structural methods. Nucleation barriers and slow diffusion were observed for all Al-Li phases. Formation of Al_2Li_3 and $AlLi_{2-x}$ appear to be linked. Rapid formation of Al_4Li_9 is very unlikely during normal cycling conditions. Elevated temperature testing offers a route to explain the apparent disconnect between electrochemical and thermal phase formation. Materials with multiple phase transitions could offer a platform for quantifying electrolyte breakdown as a function of potential and time.

Acknowledgments

Funding for this work was provided by the National Research Council Canada/University of Alberta Nanotechnology Initiative. The authors thank S. Nagy for helpful suggestions.

ORCID

Michael D. Fleischauer https://orcid.org/0000-0003-0725-2297

References

1. V. Etacheri, R. Marom, R. Elazari, G. Salitra, and D. Aurbach, *Energy & Environmental Science*, **4**, 3243 (2011).
2. W.-J. Zhang, *Journal of Power Sources*, **196**, 13 (2011).
3. L. Lu, X. Han, J. Li, J. Hua, and M. Ouyang, *Journal of Power Sources*, **226**, 272 (2013).
4. D. Lu, Y. Shao, T. Lozano, W. D. Bennett, G. L. Graff, B. Polzin, J. Zhang, M. H. Engelhard, N. T. Saenz, and W. A. J. A. E. M. Henderson, *Advanced Energy Materials*, **5**, 1400993 (2015).
5. D. Aurbach, E. Zinigrad, Y. Cohen, and H. Teller, *Solid State Ionics*, **148**, 405 (2002).
6. M. Obrovac and V. Chevrier, *Chemical Reviews*, **114**, 11444 (2014).
7. F. Wu and G. Yushin, *Energy & Environmental Science*, **10**, 435 (2017).
8. B. Neudecker, N. Dudney, and J. Bates, *Journal of The Electrochemical Society*, **147**, 517 (2000).
9. D. Fauteux and R. Koksbang, *Journal of Applied Electrochemistry*, **23**, 1 (1993).
10. B. Ji, F. Zhang, M. Sheng, X. Tong, and Y. Tang, *Advanced Materials*, **29**, 1604219 (2017).
11. Q. Y. Li, Q. C. Pan, G. H. Yang, X. L. Lin, Z. X. Yan, H. Q. Wang, and Y. G. Huang, *RSC Advances*, **5**, 85338 (2015).
12. B. Qin, S. Jeong, H. Zhang, U. Ulissi, D. Vieira Carvalho, A. Varzi, and S. Passerini, *ChemSusChem*, **12**, 208 (2019).
13. Y. Yang, B. Qiao, X. Yang, L. Fang, C. Pan, W. Song, H. Hou, and X. Ji, *Advanced Functional Materials*, **24**, 4349 (2014).
14. A. Robertson, L. Trevino, H. Tukamoto, and J. Irvine, *Journal of Power Sources*, **81**, 352 (1999).
15. T. T. Tran and M. Obrovac, *Journal of The Electrochemical Society*, **158**, A1411 (2011).
16. S. Z. El Abedin, A. Garsuch, and F. Endres, *Australian Journal of Chemistry*, **65**, 1529 (2012).
17. F. Zhang, B. Ji, X. Tong, M. Sheng, X. Zhang, C. S. Lee, and Y. Tang, *Advanced Materials Interfaces*, **3**, 1600605 (2016).
18. G. D. Kwon, E. Moyen, Y. J. Lee, J. Joe, and D. Pribat, *ACS Applied Materials*, **10**, 29486 (2018).
19. P. Qin, M. Wang, N. Li, H. Zhu, X. Ding, and Y. Tang, *Advanced Materials*, **29**, 1606805 (2017).
20. Y. Liu, N. S. Hudak, D. L. Huber, S. J. Limmer, J. P. Sullivan, and J. Y. Huang, *Nano Letters*, **11**, 4188 (2011).
21. J. Wang, I. Raistrick, and R. A. Huggins, *Journal of The Electrochemical Society*, **133**, 457 (1986).
22. R. A. Huggins, *Journal of Power Sources*, **81**, 13 (1999).
23. J. Dahn, I. Courtney, and O. Mao, *Solid State Ionics*, **111**, 289 (1998).
24. H. Okamoto, *Journal of Phase Equilibria and Diffusion*, **33**, 500 (2012).
25. M. Lindsay, G. Wang, and H. Liu, *Journal of Power Sources*, **119**, 84 (2003).
26. D. X. Liu and A. C. Co, *Journal of the American Chemical Society*, **138**, 231 (2015).
27. C. J. Wen, B. Boukamp, R. A. Huggins, and W. Weppner, *Journal of The Electrochemical Society*, **126**, 2258 (1979).
28. M. C. Lin, J. Y. Uan, and T. C. Tsai, *International Journal of Hydrogen Energy*, **37**, 13731 (2012).
29. J. Sun, R. Lv, W. Lv, Q. H. Yang, R. Amal, and D. W. Wang, *Energy Storage Materials*, **15**, 209 (2018).
30. B. Qin, T. Diemant, H. Zhang, A. Hoefling, R. J. Behm, J. Tuebke, A. Varzi, and S. Passerini, *ChemSusChem*, **12**, 2609 (2019).
31. G. Oltean, C. W. Tai, K. Edström, and L. Nyholm, *Journal of Power Sources*, **269**, 266 (2014).
32. D. Rehnlund, F. Lindgren, S. Böhme, T. Nordh, Y. Zou, J. Pettersson, U. Bexell, M. Boman, K. Edström, and L. Nyholm, *Energy & Environmental Science*, **10**, 1350 (2017).
33. N. S. Hudak and D. L. Huber, *Journal of The Electrochemical Society*, **159**, A688 (2012).
34. M. Zhang, L. Xiang, M. Galluzzi, C. Jiang, S. Zhang, J. Li, and Y. Tang, *Advanced Materials*, **31**, 1900826 (2019).
35. Panasonic data sheets are available at https://na.industrial.panasonic.com/products/batteries/rechargeable-batteries/lineup/lithium-ion.
36. R. A. Guidotti, F. W. Reinhardt, and J. Odinek, *Journal of Power Sources*, **136**, 257 (2004).
37. Saft VL 32600-125 data sheet, document 54074-2-0110 (2010).
38. X. Lin, M. Salari, L. M. R. Arava, P. M. Ajayanc, and M. W. Grinstaff, *Chem. Soc. Rev.*, **25**, 5848 (2016).
39. M.-T. F. Rodrigues, G. Babu, H. Gullapalli, K. Kalaga, F. N. Sayed, K. Kato, J. Joyner, and P. M. Ajayan, *Nature Energy*, **2**, 17108 (2017).
40. M. D. Fleischauer, M. R. Kupsta, and A. D. Johnson, *Journal of The Electrochemical Society*, **166**, A398 (2019).
41. M. H. Tahmasebi, D. Kramer, R. Mönig, and S. T. Boles, *Journal of The Electrochemical Society*, **166**, A5001 (2019).
42. Y. Geronov, P. Zlatilova, and G. Staikov, *Journal of Power Sources*, **12**, 155 (1984).
43. S. Kuksenko, *Russian Journal of Electrochemistry*, **49**, 67 (2013).
44. X. Tong, F. Zhang, B. Ji, M. Sheng, and Y. Tang, *Advanced Materials*, **28**, 9979 (2016).

45. R. Doglione, S. Vankova, J. Amici, and N. Penazzi, *Journal of Alloys and Compounds*, **727**, 428 (2017).
46. J. P. Pereira Ramos, R. Messina, and J. Perichon, *Journal of Electroanalytical Chemistry and Interfacial Electrochemistry*, **209**, 283 (1986).
47. E. Frazer, *Journal of Electroanalytical Chemistry and Interfacial Electrochemistry*, **121**, 329 (1981).
48. S. T. Myung and H. Yashiro, *Journal of Power Sources*, **271**, 167 (2014).
49. M. S. Leite, D. Ruzmetov, Z. Li, L. A. Bendersky, N. C. Bartelt, A. Kolmakov, and A. A. Talin, *Journal of Materials Chemistry A*, **2**, 20552 (2014).
50. P. Verma, P. Maire, and P. Novák, *Electrochimica Acta*, **55**, 6332 (2010).
51. R. Sarmiento Pérez, T. F. Cerqueira, I. Valencia Jaime, M. Amsler, S. Goedecker, A. H. Romero, S. Botti, and M. A. Marques, *The Journal of Chemical Physics*, **142**, 024710 (2015).
52. H.-L. Yu, X. H. Duan, Y. J. Ma, and M. Zeng, *Chinese Journal of Chemical Physics*, **25**, 659 (2012).
53. K. Puhakainen, M. Bostrom, T. L. Groy, and U. Haussermann, *J. Solid State Chem.*, **183**, 2528 (2010).